Orientational ordering of confined hard rods: The effect of shape anisotropy on surface ordering and capillary nematization

R. Aliabadi,[1,*] M. Moradi,[1,†] and S. Varga[2,‡]

[1]*Department of Physics, College of Science, Shiraz University, Shiraz 71454, Iran*
[2]*Institute of Physics and Mechatronics, University of Pannonia, PO Box 158, Veszprém H-8201, Hungary*

We examine the ordering properties of rectangular hard rods with length L and diameter D at a single planar wall and between two parallel hard walls using the second virial density-functional theory. The theory is implemented in the three-state Zwanzig approximation, where only three mutually perpendicular directions are allowed for the orientations of hard rods. The effect of varying shape anisotropy is examined at $L/D = 10, 15$, and 20. In contact with a single hard wall, the density profiles show planar ordering, damped oscillatory behavior, and a wall-induced surface ordering transition below the coexisting isotropic density of a bulk isotropic-nematic (I-N) phase transition. Upon approaching the coexisting isotropic density, the thickness of the nematic film diverges logarithmically, i.e., the nematic wetting is complete for any shape anisotropy. In the case of confinement between two parallel hard walls, it is found that the continuous surface ordering transition depends strongly on the distance between confining walls H for $H < L$, while it depends weakly on H for $H > L$. The minimal density at which a surface ordering transition can be realized is located at around $H \sim 2D$ for all studied shape anisotropies due to the strong interference effect between the two hard walls. The first-order I-N phase transition of the bulk system becomes a surface ordered isotropic I_B to capillary nematic N_B phase transition in the slit pore. This first-order I_B-N_B transition weakens with decreasing pore width and terminates in a critical point for all studied shape anisotropies.

PACS number(s): 64.70.mf, 64.60.Cn, 68.08.Bc

I. INTRODUCTION

Onsager presented a theoretical verification that anisotropic hard-body interactions are sufficient for the formation of the nematic phase when the density is sufficiently large [1]. His theoretical description was encouraged by the experimental observations of isotropic-nematic (I-N) phase separation in systems of ribbonlike vanadium pentoxide [2] and rodlike tobacco mosaic virus particles [3]. Later such a transition was also discovered in other suspensions with different particle shapes, for instance, boardlike goethite particles [4]. In the Onsager theory the Taylor expansion of the Helmholtz excess-free-energy functional is truncated at the second order and becomes exact for very long hard rods at low concentration. The theory predicts correctly the bulk I-N transition to be of first order [5].

Due to the existence of a much richer phase behavior in confined liquid crystals, the surface effects are very interesting in practical applications. For example, the walls can give rise to different anchoring phenomena and result in various phase behaviors such as a shift in the phase transition with respect to that of the bulk phase [6,7]. In general, when a liquid is located in contact with another phase, such as a solid surface, the substrate gives rise to substantial changes in the structure and the phase behavior of the liquid [8,9]. This is because of the strong competition between particle-particle (intrinsic interactions) and particle-substrate (extrinsic interactions) interactions [10]. This is especially true for mesophase forming systems, where the solid surface may change the isotropic or

nematic fluid structure from uniaxial to biaxial. It is predicted that the wall-induced uniaxial-biaxial (U-B) phase transition is continuous for confined long hard rods [11,12]. However, even the first-order U-B transition can be also found in the system of semiflexible polymers with hard-core interactions [13].

Over the past decade many experimental [14,15] and theoretical [11–17] works have supported the progress in the field of biaxial nematic phases (first prediction by Freiser [18]). The formation of a biaxial nematic film with the director parallel to the wall has been noted in colloidal hard-rod fluids near a single wall and confined between two hard walls using both theory and simulation [11,12,19]. The film wets the surface completely as the density approaches the density of the bulk I-N transition [11,12,20]. Complete wetting requires the wall-isotropic surface tension to be the sum of the wall-nematic and I-N surface tensions. This will be discussed in Sec. III. It has been also shown that the first-order capillary nematization arising from confining walls, where the I-N phase transition occurs at the lower chemical potential with respect to the bulk value [21], terminates in a capillary critical point with a narrowing of the width of the pore. The above results can be summarized as follows: (i) The wall induces a surface transition from uniaxial to biaxial symmetry, (ii) the nematic film wets completely the wall-isotropic fluid interface, and (iii) the critical wall separation at which capillary nematization terminates is about twice the length of the rod [11]. Note that similar behavior has been also seen in the system of two-dimensional hard rods in some geometric confinements [22].

In this paper we concentrate theoretically on the effects of shape anisotropy of rectangular hard rods with aspect ratios L/D of 10, 15, and 20 on the I-N interfacial tension of the I-N

*r_aliabadi@shirazu.ac.ir
†moradi@susc.ac.ir
‡vargasz@almos.uni-pannon.hu

interface, on the surface ordering and nematic wetting against a single hard wall, and on the capillary nematization and surface ordering between two parallel hard walls. In Sec. II we briefly present the Onsager theory within the Zwanzig approximation [23] where only three mutually perpendicular directions are allowed. Even though this model is simple, it captures the basic physics of the systems and also makes the numerical analysis substantially easier [11]. In Sec. III we present our numerical results and discussion. A summary is given in Sec. IV. We show a method for the location of the U-B transition in the Appendix.

II. THEORY

We study the ordering properties of rectangular hard rods with length L and diameter D in the presence of confining hard walls using the second virial theory (or Onsager theory) and the so-called three-state Zwanzig approximations for the particles' orientations. In the Zwanzig approximation, the particles' principle axes are allowed to point along one of the Cartesian axes (x, y, and z) as shown in Fig. 1, i.e., the system corresponds to a ternary mixture of hard bodies without rotational freedom. In this three-state model the grand potential of the system on the level of Onsager theory can be written as

$$
\beta\Omega = \sum_{i=x,y,z} \int d(1)\rho_i(1)\ln\rho_i(1) - \rho_i(1)
$$
$$
- \frac{1}{2}\sum_{i,j=x,y,z}\int d(1)\rho_i(1)\int d(2)\rho_j(2)f_M^{ij}(1,2)
$$
$$
+ \sum_{i=x,y,z}\int d(1)\rho_i(1)\big[\beta V_{\text{ext}}^i(1) - \beta\mu\big], \quad (1)
$$

where $\beta = 1/k_B T$, ρ_i is the local density of component i [long principle axes of particles are parallel to the i axis ($i = x,y,z$)], f_M^{ij} is the Mayer function between components i and j, V_{ext}^i is the external potential for component i, and μ is the chemical potential. The integrations are performed in positions, i.e., $(i) = d\vec{r}_i$, where $\vec{r}_i = (x_i,y_i,z_i)$ is the position vector ($i = 1,2$). Since the normal of the confining wall is parallel to the z axis (V_{ext}^i is z dependent) and we are only interested in orientational ordering transitions, the local-density components ρ_i ($i = x,y,z$) depend only on the perpendicular distance z from the wall. Using the fact that f_M^{ij}
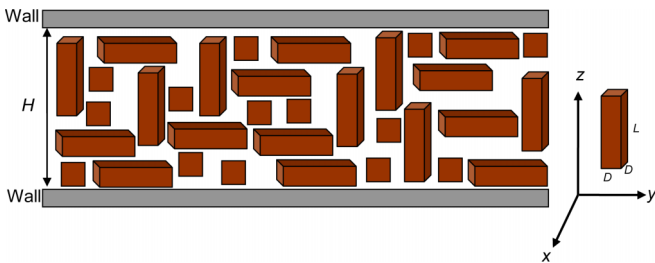

FIG. 1. (Color online) Schematic representation of the rectangular hard rods confined in a slit pore. Particles are allowed to orient along the x, y, and z axes (Zwanzig approximation). Here H is the wall-to-wall separation and L and D are the length and the diameter of hard rods, respectively.

is equal to -1 for overlapping particles and zero otherwise, we can integrate out the in-plane variables (x and y) in Eq. (1), i.e., the grand potential simplifies to

$$
\beta\Omega/A = \sum_{i=x,y,z}\int dz\rho_i(z)\ln\rho_i(z) - \rho_i(z)
$$
$$
+ \frac{1}{2}\sum_{i,j=x,y,z}\int dz_1\rho_i(z_1)\int dz_2\rho_j(z_2)A_{\text{exc}}^{ij}(z_{12})
$$
$$
+ \sum_{i=x,y,z}\int dz_1\rho_i(z_1)\big[\beta V_{\text{ext}}^i(z_1) - \beta\mu\big], \quad (2)
$$

where A is the surface of the confining walls, $A_{\text{exc}}^{ij}(z) = -\int dx \int dy\, f_M^{ij}$ is the excluded area between two hard particles with orientations i and j ($i,j = x,y,z$), and $z_{12} = z_1 - z_2$ is the vertical distance between two rods, respectively. For rectangular hard rods with length L and cross section lengths D, the excluded areas can be determined analytically and are given by

$$
A_{\text{exc}}^{xx}(z) = A_{\text{exc}}^{yy}(z) = 4DL \quad \text{for} -D < z < D,
$$
$$
A_{\text{exc}}^{zz}(z) = 4D^2 \quad \text{for} -L < z < L,
$$
$$
A_{\text{exc}}^{xy}(z) = A_{\text{exc}}^{yx}(z) = (L+D)^2 \quad \text{for} -D < z < D,
$$
$$
A_{\text{exc}}^{xz}(z) = A_{\text{exc}}^{zx}(z) = A_{\text{exc}}^{yz}(z) = A_{\text{exc}}^{zy}(z) = 2D(L+D) \quad \text{for}
$$
$$
-\frac{L+D}{2} < z < \frac{L+D}{2}. \quad (3)
$$

Note that the above excluded areas are symmetric, i.e., $A_{\text{exc}}^{ij} = A_{\text{exc}}^{ji}$, and zero if the z distance between the two particles is outside the indicated intervals. The external potential of the system confined between two parallel walls is purely hard and defined for parallel and perpendicular particle orientations to the walls as follows:

$$
\beta V_{\text{ext}}^i(z) = \begin{cases} \infty, & z < D/2, \quad z > H - D/2 \\ 0, & D/2 < z < H - D/2 \end{cases} \quad (i = x,y),
$$
$$
\beta V_{\text{ext}}^z(z) = \begin{cases} \infty, & z < L/2, \quad z > H - L/2 \\ 0, & L/2 < z < H - L/2, \end{cases} \quad (4)
$$

where H is the distance between the two parallel walls. In the case of single wall, since the wall is located at $z = 0$, the external potential is infinite only for distances below $D/2$ and $L/2$ in the above expressions, respectively. The equilibrium local densities are obtained from the functional minimization of the grand potential with respect to the local densities, i.e., $\frac{\delta\beta\Omega/A}{\delta\rho_k(z)} = 0$. The resulting three integral equations can be written concisely as

$$
\rho_i(z) = \exp\left\{-\sum_{j=x,y,z}\int dz_1\rho_j(z_1)A_{\text{exc}}^{ij}(z - z_1)\right\}
$$
$$
\times \exp\{-\beta V_{\text{ext}}^i(z)\}\exp\{\beta\mu\} \quad (i = x,y,z). \quad (5)
$$

It can be seen that Eq. (5) corresponds to three self-consistent and coupled equations for the local densities ρ_x, ρ_y, and ρ_z at a given chemical potential (μ). We have solved Eq. (5)

by the standard iteration method and used the trapezoidal quadrature for the calculations of the integrals. Although the x and y orientations are equivalent, we have chosen such trial distribution functions for the local densities, which may result in solutions such that $\rho_x \geqslant \rho_y$. In the bulk phase, where the external potential term is missing, the above coupled equations become much simpler, because the local densities lose their positional dependence. From Eq. (5) one can derive that

$$\rho_i = \exp\left[-\sum_{j=x,y,z} \rho_j V_{\text{exc}}^{ij}\right]\exp[\beta\mu] \quad (j = x,y,z), \quad (6)$$

where $V_{\text{exc}}^{ij} = \int dz\, A_{\text{exc}}^{ij}(z)$ is the excluded volume between two rods. In this case only parallel and perpendicular orientations can be distinguished, i.e., $V_{\text{exc}}^{\parallel} = V_{\text{exc}}^{ii} = 8LD^2$ ($i = x,y,z$) and $V_{\text{exc}}^{\perp} = V_{\text{exc}}^{ij} = 2D(L+D)^2$ ($i = \neq j$). In bulk one of the solutions of Eq. (6) is isotropic, i.e., $\rho_x = \rho_y = \rho_z$, while the other solution is nematic, where $\rho_x > \rho_y = \rho_z$. In the confined situation three different solutions can be obtained, one is isotropic, while the other two are orientationally ordered phases. To characterize the type and the degree of ordering we use three different orientational order parameters. One of them is the orientation average of the second Legendre polynomial if the director is chosen to be along the x axis, i.e., $S_x = \langle P_2 \rangle_{\vec{n}=(1,0,0)}$, while the other order parameters Δ_{xy} and Δ_{yz} measure the degree of biaxiality between two in-plane orientations (x and y) and between one in-plane and one out-of-plane orientation (y and z). In our approach the formulas for these order parameters are

$$S_x = \frac{\rho_x - \rho_y/2 - \rho_z/2}{\rho}, \quad (7)$$

$$\Delta_{xy} = \frac{\rho_x - \rho_y}{\rho}, \quad (8)$$

and

$$\Delta_{yz} = \frac{\rho_y - \rho_z}{\rho}, \quad (9)$$

where $\rho = \rho_x + \rho_y + \rho_z$ is the total local density. In the bulk isotropic phase all these order parameters are zero, while $0 < S_x < 1$ and one of the biaxial order parameters is zero (either $\Delta_{xy} = 0$ or $\Delta_{yz} = 0$) in the bulk nematic phase. In the case of confined systems the local densities are not constant and the confining walls induce planar ordering in the vicinity of the walls even for arbitrary small chemical potentials. Therefore, the isotropic phase of confined systems has the property that $S_x \geqslant 0$ and only one biaxial order parameter is nonzero ($\Delta_{yz} > 0$ and $\Delta_{xy} = 0$), which corresponds to the case when $\rho_x = \rho_y > \rho_z$. The other phase is also isotropic to some extent, but surface ordering takes place in the vicinity of the walls, i.e., the phase is biaxial at the walls. In this case the local densities are nonequal in the vicinity of walls ($\rho_x > \rho_y > \rho_z$), but $\rho_x = \rho_y \geqslant \rho_z$ happens far from the walls. This corresponds to $S_x > 0$ and $\Delta_{xy}, \Delta_{yz} > 0$ close to the walls, while $\Delta_{xy} = 0$ far from the walls. The nematic phase is biaxial at the walls, i.e., $S_x > 0$ and $\Delta_{xy}, \Delta_{yz} > 0$, but it becomes differently uniaxial far from the walls due to $\rho_x > \rho_y = \rho_z$ ($\Delta_{xy} > 0$ and $\Delta_{yz} = 0$) if the pore is very wide. We present the local-density and order-parameter curves of different structures in the next section. Since both first- and second-order phase transitions may occur in confined systems, we undertake a bifurcation analysis between uniaxial and biaxial phases and determine the coexisting densities of different phases. In our case the bifurcation analysis, which is presented in the Appendix, gives the phase boundary of the surface ordering phase transition since this transition is of second order. The properties of the first-order phase transitions in both the bulk and confined cases, which take place between isotropic and nematic phases, are determined by searching the intersection between two different solutions of Eq. (5) in the $\beta\Omega/A$-$\beta\mu$ plane.

The calculated equilibrium density profiles can be also used to determine the interfacial surface tensions (γ_{WI}, γ_{WN}, and γ_{IN}). These profiles are inserted into Eq. (2) to get the equilibrium value of the grand potential Ω_0 of the system. All surface tensions have been calculated using the general definition of the surface tension as the surface excess grand potential per unit area

$$\gamma = \frac{\Omega_0 + pV}{A}, \quad (10)$$

where p is the pressure and V is the volume of the system. In the figures dimensionless number densities $\rho^* = \rho D^3$, pore width $h^* = H/D$, and vertical position $z^* = z/D$ are utilized.

III. RESULTS AND DISCUSSION

Prior to the study of the structure and phase behavior of the confined hard-rod fluid we have calculated the homogeneous bulk I-N phase boundary, as shown in Fig. 2, by searching for the intersection between two different solutions of Eq. (6) in $\beta\Omega/A$-$\beta\mu$ plane. Figure 2 shows that the I-N phase
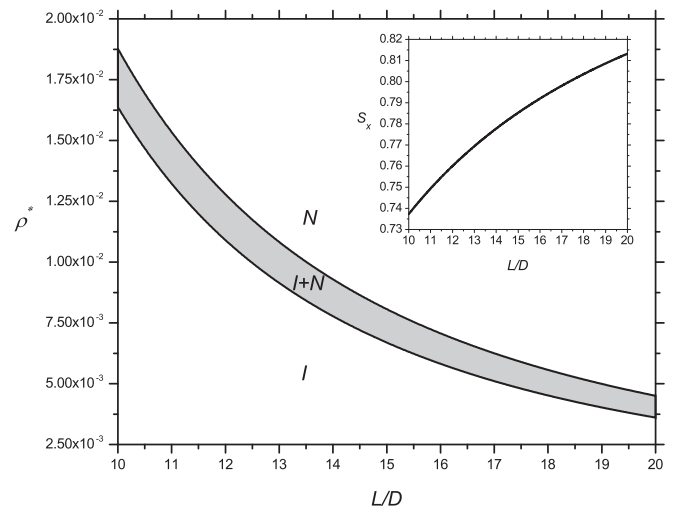

FIG. 2. Isotropic-nematic phase boundary of hard rods in bulk. Coexisting isotropic I and nematic N densities are shown as a function of aspect ratio L/D. The inset depicts the nematic order parameter S_x of the coexisting nematic phase. Here ρ^* is the reduced number density ($\rho^* = \frac{N}{V}D^3$).
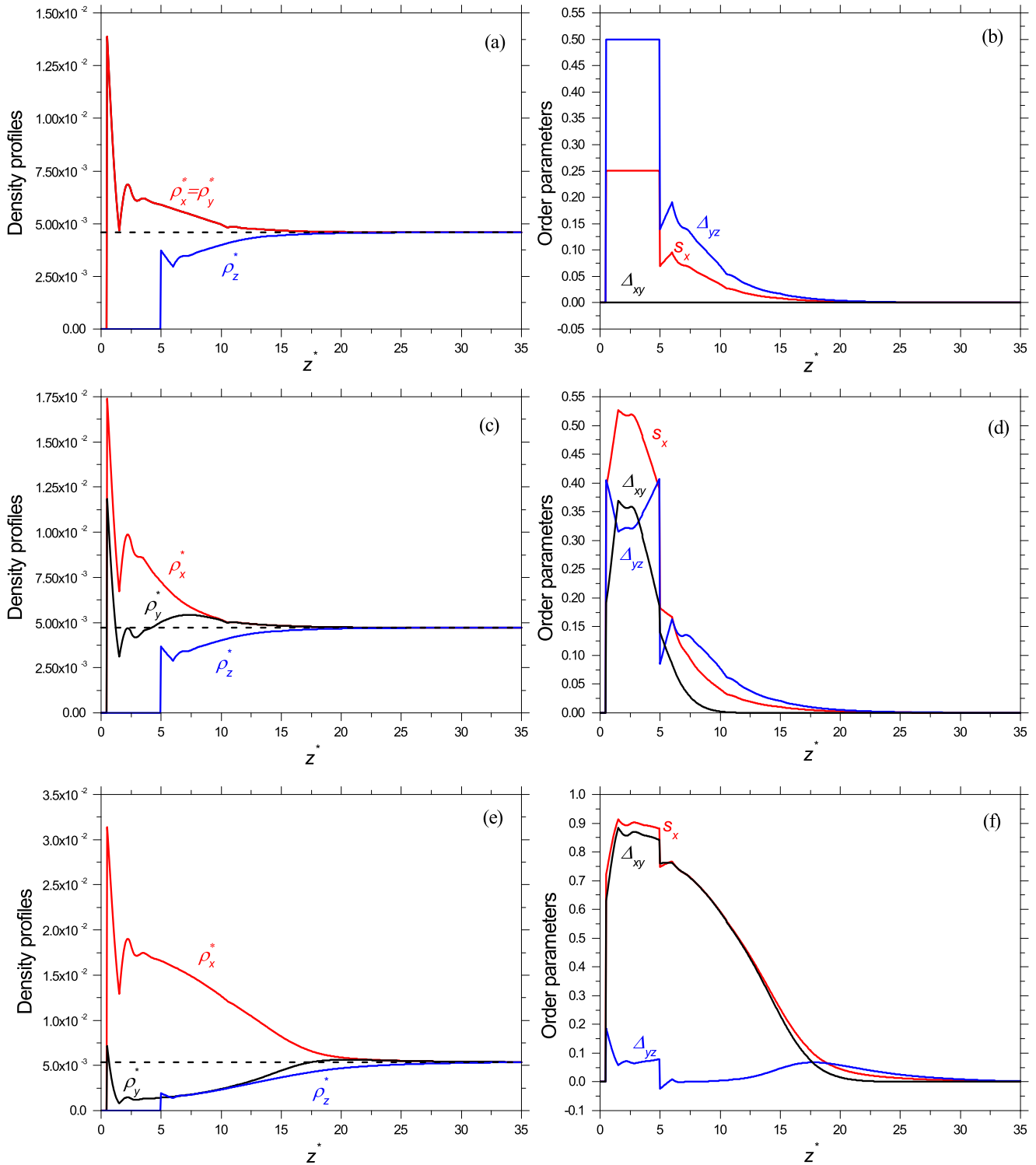
FIG. 3. (Color online) Density profiles and order parameters of the hard rod fluid in contact with a single hard wall that is located at $z^* = 0$. The aspect ratio L/D is chosen to be 10. (a) and (b) Obtained at $\beta\mu = -2.8$, where the phase is isotropic and the bulk component densities (dotted line) are equal to 4.584×10^{-3}. (c) and (d) The case $\beta\mu = -2.7$. This phase is biaxial isotropic and the corresponding bulk component densities (dotted line) are 4.712×10^{-3}. (e) and (f) The reduced chemical potential is -2.2, where the bulk component densities are 5.368×10^{-3}.

transition is weakly first order and the coexisting densities decrease with increasing shape anisotropy. In the inset of Fig. 2 one can see that the orientational order parameter of the coexisting nematic phase increases with increasing L/D.

Apart from the shift in the coexisting densities, these results are in good agreement with the theoretical and simulation results obtained for freely rotating hard rods. This means that the three-state Zwanzig approximation represents correctly the

orientational freedom of the particles. Using Fig. 2, one can see the reference values for our confined results in the interval $10 < L/D < 20$.

In Fig. 3 we exhibit density profiles and the corresponding order parameters of the particles with $L/D = 10$ in contact with a single hard wall for three different chemical potentials where the hard planar wall is located at $z^* = 0$. The presented density profiles show a sharp and high first peak with a large contact value of ρ_x^* for all chemical potentials, i.e., there is strong adsorption at the wall. In addition to this the density profiles exhibit damped oscillatory behavior near the planar wall, while they converge to the bulk density values far from the wall. Near the surface ρ_z^* is always smaller than $\rho_b^*/3$, while ρ_x^* is always higher at any distance for all chemical potentials shown. This shows that the ordering is planar at the wall. The phase is isotropic with planar order at $\beta\mu = -2.8$, as can be seen from Figs. 3(a) and 3(b), where ρ_x^* is equal to ρ_y^*, i.e., surface induced biaxiality is not present ($\Delta_{xy} = 0$). Sufficiently far from the wall all densities approach the bulk density ($\rho_b^*/3 = 4.584 \times 10^{-3}$). As the chemical potential is increased biaxial order starts to exist as the number of particles parallel to the x axis increases more than the number of particles parallel to the y axis. In Figs. 3(c) and 3(d), $\rho_x^* \neq \rho_y^*$ and Δ_{xy} and Δ_{yz} are nonzero spontaneously near the wall, so the phase is biaxial. These figures show surface ordering and formation of a nematic film. In Fig. 3(e), where the chemical potential is chosen to be close to $\beta\mu_{IN}^b \approx -2.1327$, a substantial increase in the value of ρ_x^* can be seen with respect to ρ_y^* and ρ_z^*. This indicates that the thickness of the nematic layer can be grown by increasing the chemical potential. This fact is also clear from the order parameters presented in Fig. 3(f). There is a very weak negative oscillation in Δ_{yz} where $\rho_y^* < \rho_z^*$ in Fig. 3(f) right after $z^* = 5$ that becomes slightly positive before decaying quickly to zero ($\rho_y^* = \rho_z^*$). Furthermore, Δ_{yz} becomes smaller for larger chemical potentials, which means that the values of ρ_z^* and ρ_y^* are getting closer to each other. At very large distances all densities become identical, i.e., the phase is isotropic far from the wall. The wall-induced U-B transition occurs at $\beta\mu = -2.7550$, which is below the chemical potential of the bulk I-N transition ($\beta\mu_{IN}^b$). Upon getting close to $\beta\mu_{IN}^b$, the thickness of the nematic film diverges logarithmically. It is important to note that the nematic wetting is complete for any shape anisotropy as it is proved by the results for surface tensions. In summary, Fig. 3 shows that how the second-order biaxial surface ordering transition evolves with increasing chemical potential.

For some aspect ratios, the surface tensions have been calculated using Eq. (10) by choosing very large distance between the wall and the bulk fluid and between coexisting isotropic and nematic phases ($\sim 1000D$). In the case of wall-isotropic surface tension calculations, we have performed an extrapolation $\gamma_{IW}(\mu_{IN}^b) = \lim_{\mu \to \mu_{IN}^b} \gamma_{IW}(\mu)$ because the thickness of the nematic film diverges at $\beta\mu = \beta\mu_{IN}^b$. The resulting surface tensions are fitted by R^2 larger than 0.98 to a power law $\gamma^*(x) = ax^b$, where $x = L/D$. Figure 4 presents the dimensionless wall-isotropic ($\gamma_{WI}^* = \beta\gamma_{WI}D^2$), wall-nematic ($\gamma_{WN}^* = \beta\gamma_{WN}D^2$), and I-N ($\gamma_{IN}^* = \beta\gamma_{IN}D^2$) surface tensions as a function of L/D, which are given by the following fitting
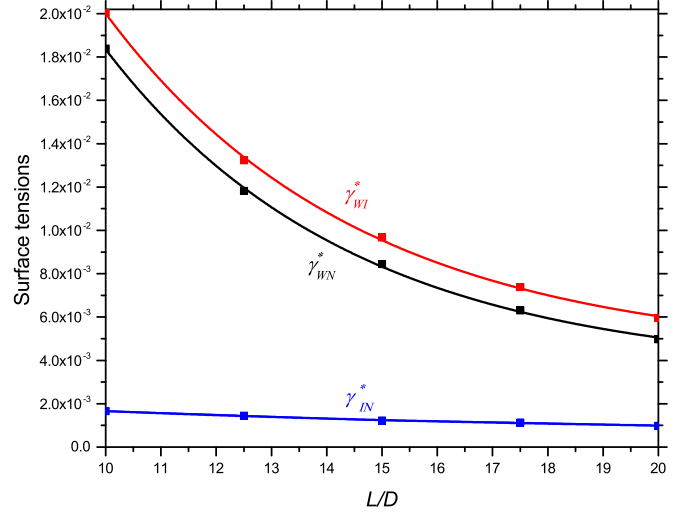

FIG. 4. (Color online) Fitted surface tensions γ_{WI}, γ_{WN}, and γ_{IN} of the hard-wall–isotropic, hard-wall–nematic, and I-N fluid interfaces, respectively. The calculated surface tensions (solid squares) are fitted by the power law $\gamma(x) = ax^b$ (solid lines), where $x = L/D$. The surface tensions are dimensionless quantities, i.e., $\gamma_{WI}^* = \beta\gamma_{WI}D^2$, $\gamma_{WN}^* = \beta\gamma_{WN}D^2$, and $\gamma_{IN}^* = \beta\gamma_{IN}D^2$.

parameters:

$$a = 1.203\,344\,132\,6, \quad b = -1.780\,189\,480\,1;$$
$$a = 1.484\,769\,749\,4, \quad b = -1.908\,806\,448\,1;$$
$$a = 0.008\,151\,231\,2, \quad b = -0.696\,668\,512\,4$$

for γ_{WI}^*, γ_{WN}^*, and γ_{IN}^*, respectively. Note that our fitting is not valid for infinitely long rods. Our results prove that the nematic wetting of the wall-isotropic fluid interface is complete by a nematic film, where the nematic director of the film is oriented parallel to the wall (x axis in our calculation). Applying the above parameters, one can find that γ_{IN} is equal to $\gamma_{WI} - \gamma_{WN}$. Therefore, the contact angle must be zero, which is apparent from Young's equation $\gamma_{IN}\cos\theta = \gamma_{WI} - \gamma_{WN}$. One can also show that the excess adsorption diverges logarithmically at $\beta\mu = \beta\mu_{IN}^b$, which is a feature of complete wetting of classical fluids interacting with short-range forces [24]. Similar behavior is reported in the Monte Carlo simulation study of hard spherocylinders [19]. It is also consistent with the profiles displayed in Fig. 3, which show an increase in the thickness of the film with increasing chemical potential. As discussed before, the wetting transition is second order.

The density profiles and order parameters of the confined fluid by two planar hard walls are based on the numerical solution of the Euler-Lagrange equation [Eq. (5) combined with Eq. (4)]. The results are presented in Fig. 5 for $L/D = 10$ at three different chemical potentials. In connection with single-hard-wall density profiles (Fig. 3), here it is also obvious that uniaxial phase changes to biaxial and most of the particles align parallel to the x axis by increasing the chemical potential. Therefore, a biaxial nematic layer forms in the whole range of the pore. Here both walls act in the same way and support the formation of the nematic film with oscillatory density profiles. At some separations both walls strengthen the biaxial order (they are in-phase), but they can weaken it at other separations
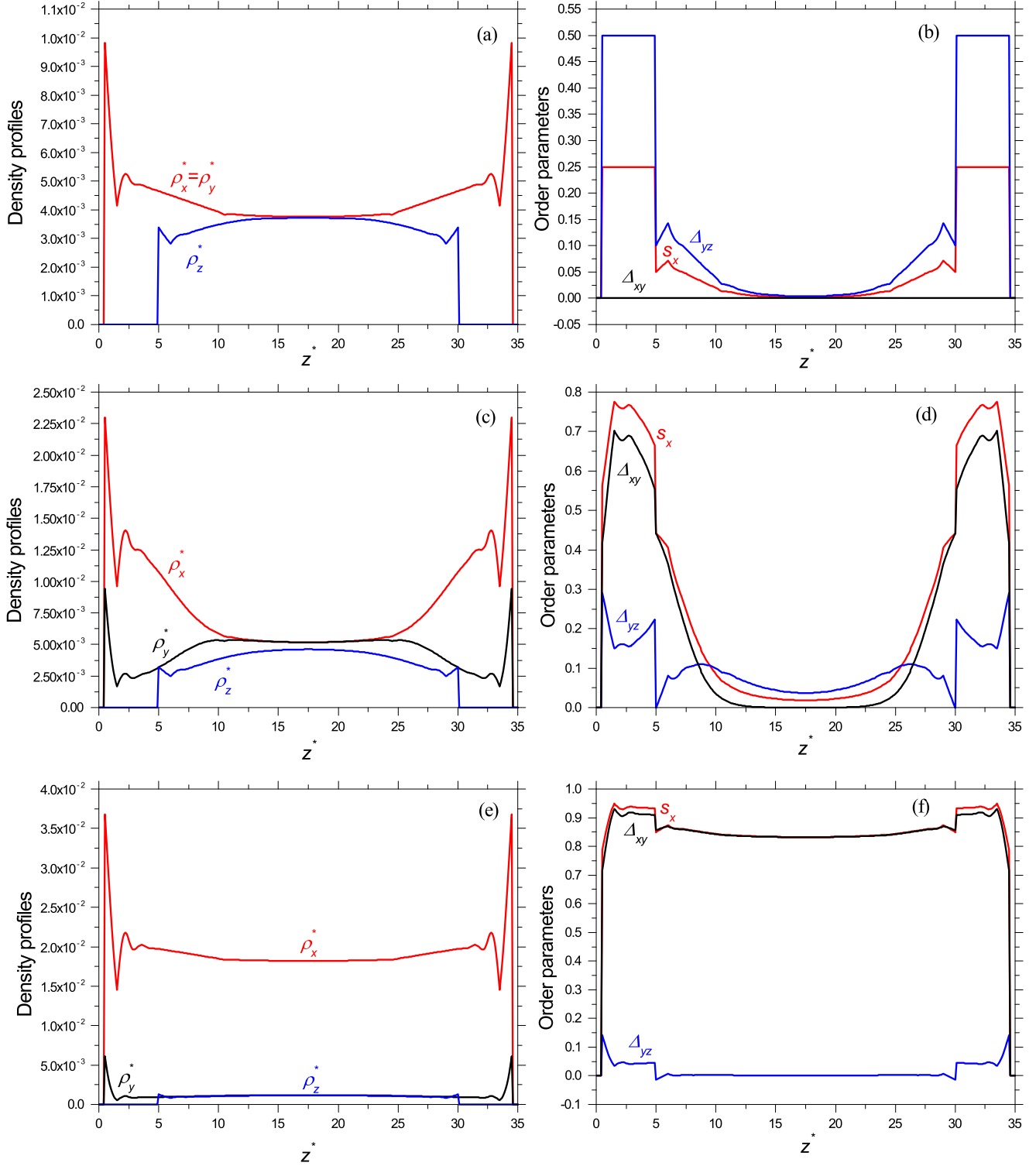
FIG. 5. (Color online) Density profiles and order parameters of confined hard rods ($L/D = 10$) between two hard walls at reduced wall separation $h^* = H/D = 35$. (a) and (b) Obtained at $\beta\mu = -3.48$, where the phase is isotropic. (c) and (d) The case $\beta\mu = -2.51$, where the phase is biaxial near the walls ($\rho_x^* \neq \rho_y^*$) but isotropic in the middle of the pore. (e) and (f) The reduced chemical potential is -2, where the phase is biaxial nematic.

(they are out of phase). Therefore, the appearance of the biaxial order in the vicinity of the walls is the result of the interference of the two walls. As can be seen from Figs. 5(a) and 5(b), the phase is isotropic at $\beta\mu = -3.48$ where ρ_x^* and ρ_y^* are equal

even close to the walls and hence $\Delta_{xy} = 0$ while $\Delta_{yz} \neq 0$ and $S_x \neq 0$ except in the middle of the pore. The phase is biaxial isotropic (or more precisely weakly nematic) for $\beta\mu = -2.51$ due to ρ_x^* and ρ_y^* being different near the surfaces but
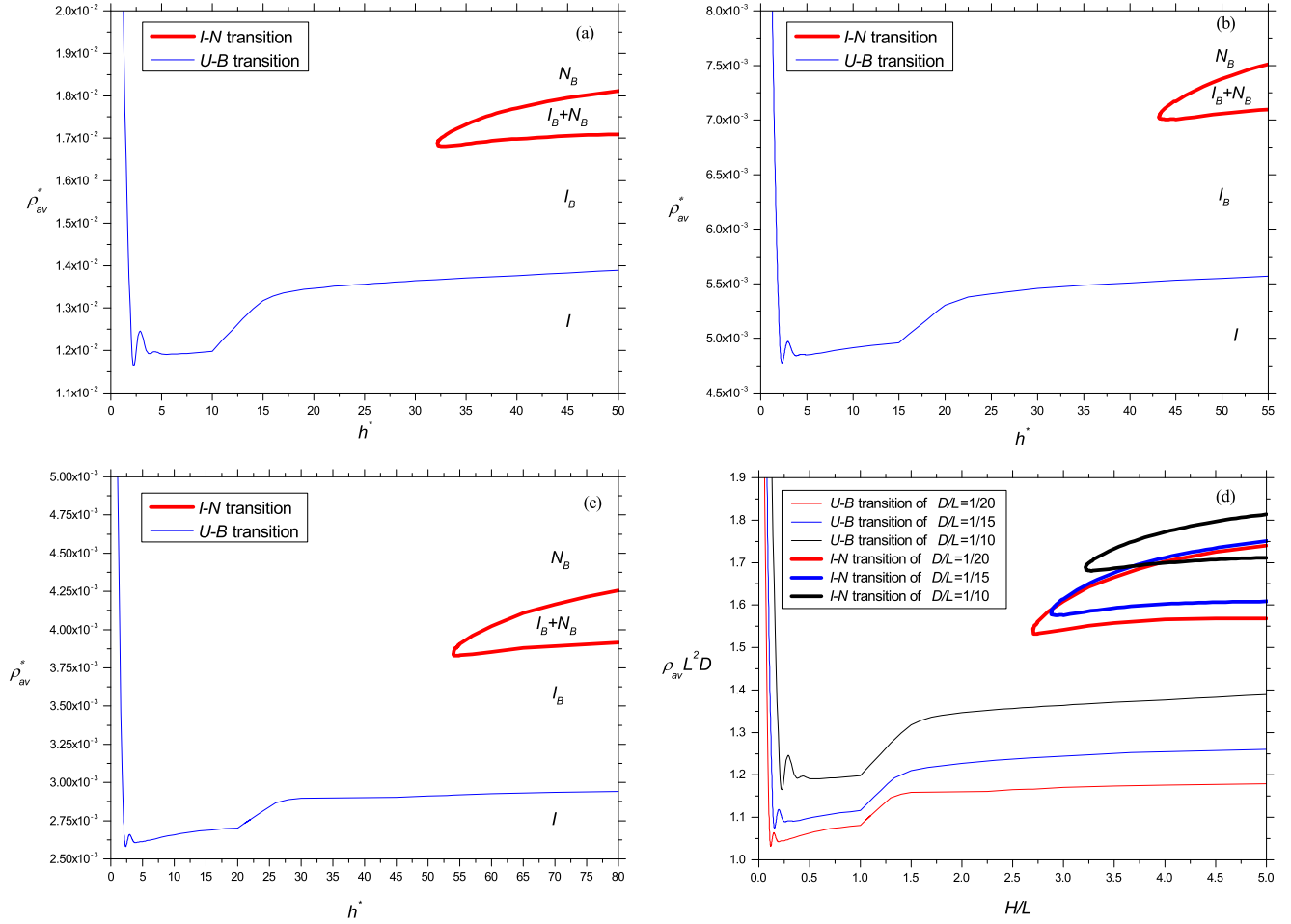
FIG. 6. (Color online) Phase diagram of confined hard rods in the density–wall-to-wall separation plane. The I_B-N_B (thick lines) and U-B (thin lines) phase transition curves are shown. The values of the aspect ratios are (a) $L/D = 10$, (b) $L/D = 15$, and (c) $L/D = 20$. The resulting phase diagrams are shown together in different units in (d).

equal in the middle of the pore [Fig. 5(c)]. In this phase, apart from the central region, $\Delta_{xy} \neq 0$ but Δ_{yz} and S_x are nonzero everywhere [Fig. 5(d)]. Moreover, S_x shows a very weak nematic ordering in the middle of the pore. The phase in Fig. 5(e) is nematic biaxial ($\beta\mu = -2.00$) since $\rho_x^* > \rho_y^*$ and most of the particles are aligned in the direction of the x axis. The nematic film persists throughout the central region. In this phase, the order parameters Δ_{xy} and S_x have large values whereas Δ_{yz} is very small due to the small difference between ρ_y^* and ρ_z^* [Fig. 5(f)].

Based on the numerical solution of Eq. (5), we have found both biaxial isotropic and biaxial nematic solutions at some values of the chemical potential, which indicates that first-order phase transitions occur in the slitlike pore. The resulting first-order phase transitions between biaxial isotropic and nematic phases (I_B-N_B) and the surface ordering transitions (U-B) are presented in a common phase diagram for different particles' shapes ($L/D = 10, 15,$ and 20) in Fig. 6. In this figure the average density in the slit pore $\rho_{av}^* = \frac{1}{H}\int_0^H \rho^*(z)dz$ is shown as a function of the reduced pore width ($h^* = H/D$). The U-B transition is always second order like the one-wall case for any shape anisotropy and oscillates with varying pore width for short pore widths. This means that

this transition strongly depends on the wall-to-wall distance if $h^* < L/D$. For more elongated particles, the heights of the waves get smaller and the transition occurs at smaller densities. When $h^* > L/D$, the U-B line becomes smoothly varying and approaches the single-wall limit of the surface ordering transition. This is due to the fact the walls are too far from each other and the interference weakens between them. The first-order I-N transition of the bulk system becomes a surface ordered I_B-N_B phase transition in the slit pore. This first-order I_B-N_B transition weakens with decreasing pore width and terminates at a critical (capillary) point h_c^* for all studied shape anisotropies similar to the studies for infinitely long hard rods [11,12] and finite rods [19]. As a result, the two coexisting biaxial phases become fully indistinguishable as $h^* \to h_c^{*+}$. The N_B and I_B phases are less and less biaxial far from the walls if H goes to infinity. The I_B-N_B coexistence densities in the pores are smaller in comparison with their bulk I-N densities (see Fig. 2) because the planar walls promote the formation of nematic ordering. These coexisting densities of the confined system approach the bulk I-N coexisting densities with increasing pore width. The critical points for particles with $L/D = 10$ and 15 are located at $h_c^* = 32.1605$ and 43.1630, respectively. A similar result has been reported
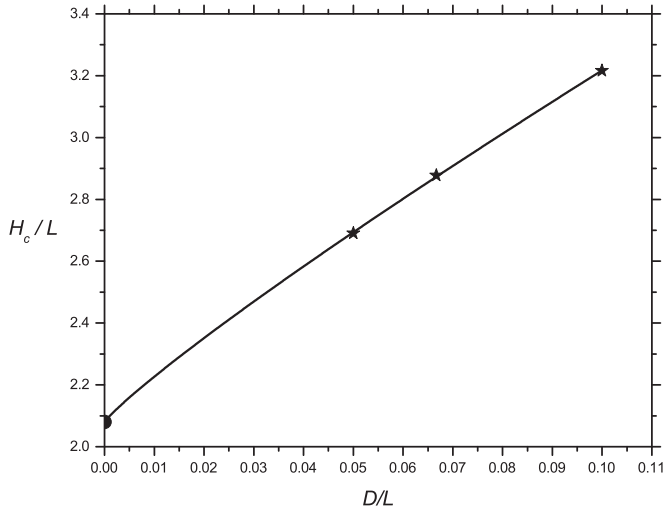
FIG. 7. Critical pore width H_c/L as a function of D/L. The stars correspond to our numerical results, while the closed circle is the result of van Roij *et al.* for $D/L \rightarrow 0$ [11]. The fitted equation (solid line) is given by $H_c/L = 2.08\,(1 + ax^b)$, where $x = D/L$, $a = 4.248\,57$, and $b = 0.890\,38$.

rods with shape anisotropies of $L/D = 10,15$, and 20 have been considered in contact with a single planar hard wall and in confinement where the rods are constrained to stay between two parallel hard walls. In the first part of the study we calculated bulk coexisting I-N densities as a function of L/D. It was found that the Zwanzig approximation, which is widely used for both bulk [25] and confined systems [26], does not change qualitatively the results for the I-N coexisting densities and order parameters, i.e., it shows decreasing transition densities and increasing order parameters with increasing L/D, in agreement with the theoretical results obtained for freely rotating hard rods. In the case of a single hard wall, we have found that the uniaxial phase changes to the biaxial one near the wall as the chemical potential is increased. Wall-induced planar surface ordering and the formation of a biaxial nematic film parallel to the wall have been observed for all shape anisotropies. The planar ordering is thermodynamically more favorable than the homeotropic ordering, where the nematic director is perpendicular to the wall. The thickness of the nematic film diverges logarithmically, as is expected for systems interacting with short-range forces. The three surface tensions calculated were fitted well by asymptotic functions. They show a zero contact angle, which means that the nematic layer wets the wall-isotropic interface completely for any shape anisotropy.

In the second part of this study we considered the fluid of hard rods confined between two parallel hard walls. It was found that the increasing chemical potential stabilizes the biaxial nematic film that persists throughout the pore. There is a continuous surface ordering transition from uniaxial to biaxial symmetry with smoothly varying transition density that is below the bulk I-N coexistence densities for $h^* > L/D$, while the surface ordering transition density oscillates and depends strongly on the wall-to-wall separation for $h^* < L/D$. The weak and the strong h^* dependence of the surface ordering transition density is due to the weak and strong interference of the two wall-induced orderings. We have found a first-order capillary I_B nematization transition that terminates at a critical pore width h_c^* for any shape anisotropy. Our study reveals the difference between the ordering properties of hard rods in narrow and wide pores. Only a surface ordering transition takes place in narrow pores because the system is reminiscent of quasi-two-dimensional systems of hard rods, where the ordering transition is continuous [27]. In wider pores both surface ordering transitions and capillary nematization are present due to the strong adsorption at the walls and the competition between packing and orientational entropies. These transitions occur even at infinite pore width ($h^* \rightarrow \infty$), where the walls do not effect the I-N properties, i.e., the coexisting densities of the I_B and N_B phases become identical to those of the bulk I-N transition. In comparison with previous theoretical results [11,12], our study shows that the Onsager theory is able to result in richer local structures for the confined isotropic and nematic phases and to describe the oscillatory behavior of the surface ordering transition if all terms of the excluded-volume interactions are incorporated into the calculations.

As an extension of our present work we plan to study the ordering properties of board-shaped hard rods, where the cross-section lengths are different ($D_1 < D_2 < L$). This would

for a fluid of hard spherocylinders with a length-to-diameter ratio of 15 by a simulation study [19]. The critical point for particles with $L/D = 20$ is close to $h_c^* \approx 54$ (we have not managed to determine it more accurately). Using L as a unit of distance and $\rho_{av}L^2D$ as a dimensionless density, the transition densities of the $L/D = 10,15$, and 20 cases become of the same order of magnitude and the phase diagrams can be shown together in the $\rho_{av}L^2D$-H/L plane [see Fig. 6(d)]. The main advantage of this representation is that it is possible to make a connection with the well-known Onsager limit ($L/D \rightarrow \infty$). One can see that the U-B surface ordering transition becomes less oscillatory and it is shifted in the direction of the limiting value of $\rho_{av}L^2D \approx 1.031$, which is obtained for the $L/D \rightarrow \infty$ case [11,12]. It can also be seen that the critical pore width of the $I_B - N_B$ transition gets closer to the limiting value of $H_c/L = 2.08$ with increasing aspect ratio. Figure 7 shows the relationship between the calculated $I_B - N_B$ critical points and D/L. To see the correction of the finite aspect ratio, we make the following fit for the critical pore width: $H_c/L = 2.08\,(1 + ax^b)$, where $x = D/L$. This formula reproduces the $L/D \rightarrow \infty$ case exactly, where $H_c/L = 2.08$. One can see that our fitting formula with the values $a = 4.248\,75$ and $b = 0.890\,38$ reproduces quite accurately the numerical results. The reason why an even more than 50% difference emerges between the H_c/L of the $L/D = 10$ and $L/D \rightarrow \infty$ cases is that the terms A_{exc}^{ii} are not negligible and become more dominant at lower aspect ratios.

IV. CONCLUSION

In this work we have studied the influence of shape anisotropy of rectangular hard rods on the structural properties and phase behavior of isotropic and nematic phases in the presence of confinement using Onsager's well-known second virial theory with three-state restriction for the orientations of hard rods (the Zwanzig approximation). Fluids of hard

allow us to study the phase behavior of confined goethite nanorods, which has proven to be the first colloidal system showing biaxial nematic ordering [28–31]. Along this line, the effects of shape polydispersity and the external magnetic field on the stability of biaxial nematic phase have already been the subject of recent theoretical and experimental studies [32,33].

APPENDIX: BIFURCATION ANALYSIS OF THE SURFACE ORDERING TRANSITION

The simplest method of finding the second-order transition point between disordered and ordered phases at the surfaces is to decrease the chemical potential with fine steps. At high chemical potentials we obtain ordered solutions with $\Delta_{xy} \neq 0$ and $\Delta_{yz} \neq 0$ close to the walls, while Δ_{xy} becomes zero at the transition point. Instead of decreasing the chemical potential and looking at the value of Δ_{xy} when it becomes zero, we present here an elegant method for the location of the surface ordering transition.

In the isotropic phase of confined hard particles the in-plane local densities are identical while the out-of-plane one is different [$\rho_x(z) = \rho_y(z) \neq \rho_z(z)$]. Assuming that the biaxial order evolves continuously from the isotropic one, we apply the following ansatz for the biaxial order:

$$\hat{\rho}_x(z) = \rho_x(z)[1 + \varepsilon(z)],$$
$$\hat{\rho}_y(z) = \rho_y(z)[1 - \varepsilon(z)], \qquad \text{(A1)}$$
$$\hat{\rho}_z(z) = \rho_z(z),$$

where $\varepsilon(z)$ is an unknown biaxial perturbation. Note that $\rho_x(z)$, $\rho_y(z) = \rho_x(z)$, and $\rho_z(z)$ are the isotropic solution of Eq. (5).

Since Eq. (A1) also satisfies Eq. (5), we get that the biaxial perturbation obeys the equation

$$1 + \varepsilon(z) = \exp\left\{ -\int_{\max(D/2, z-D)}^{\min(H-D/2, z+D)} dz'\varepsilon(z')\rho_x(z')A_{\text{exc}}^{xx} \right.$$
$$\left. + \int_{\max(D/2, z-D)}^{\min(H-D/2, z+D)} dz'\varepsilon(z')\rho_x(z')A_{\text{exc}}^{xy} \right\}, \quad \text{(A2)}$$

where $A_{\text{exc}}^{xx} = 4LD$ and $A_{\text{exc}}^{xy} = (L + D)^2$. After linearization of the exponential function $\exp(x) \approx 1 + x$ and the rearrangement of Eq. (A2) we get that

$$\int_{\max(D/2, z-D)}^{\min(H-D/2, z+D)} dz'\varepsilon(z')\left\{\delta(z - z') + \left[A_{\text{exc}}^{xx} - A_{\text{exc}}^{xy}\right]\rho_x(z')\right\}$$
$$= 0, \qquad \text{(A3)}$$

where $\delta(z)$ is the Dirac delta function. Formally Eq. (A3) can be satisfied with $\varepsilon(z) \neq 0$ if the determinant of the argument vanishes, i.e.,

$$\det\left|\delta(z - z') + \left[A_{\text{exc}}^{xx} - A_{\text{exc}}^{xy}\right]\rho_x(z')\right| = 0. \qquad \text{(A4)}$$

In practice, we have produced a matrix using the discretized values of the local density of the isotropic solution of Eq. (5) and we have searched for that chemical potential at which the local density satisfies both Eqs. (A4) and (6). Results from Eq. (A4) and the method of decreasing chemical potential agree perfectly. The main advantage of our method is that we do not have to determine the biaxial perturbation $\varepsilon(z)$.

[1] L. Onsager, Ann. N.Y. Acad. Sci. **51**, 627 (1949).

[2] H. Zocher, Z. Anorg. Chem. **147**, 91 (1925).

[3] F. C. Bawden, N. W. Pirie, J. D. Bernal, and I. Fankuchen, Nature (London) **138**, 1051 (1936).

[4] k. Coper and H. Freundlich, T. Faraday Soc. **33**, 348 (1937).

[5] H. Reich, M. Dijkstra, R. van Roij, and M. Schmidt, J. Phys. Chem. B **111**, 7825 (2007).

[6] A. Malijevsky and S. Varga, J. Phys.: Condens. Matter **22**, 175002 (2010).

[7] P. Sheng, Phys. Rev. Lett. **37**, 1059 (1976).

[8] P. I. C. Teixeira and T. J. Sluckin, J. Chem. Phys. **97**, 1498 (1992).

[9] M. Moradi, R. J. Wheatley, and A. Avazpour, Phys. Rev. E **72**, 061706 (2005).

[10] D. de las Heras, E. Velasco, and L. Mederos, Phys. Rev. E **74**, 011709 (2006).

[11] R. van Roij, M. Dijkstra, and R. Evans, J. Chem. Phys. **113**, 7689 (2000).

[12] R. van Roij, M. Dijkstra, and R. Evans, Europhys. Lett. **49**, 350 (2000).

[13] Z. Y. Chen and S. M. Cui, Phys. Rev. E **52**, 3876 (1995).

[14] P. A. Santoro, A. R. Sampaio, H. L. F. da Luz, and A. J. Palangana, Phys. Lett. A **353**, 512 (2006).

[15] D. A. Oliveira, D. D. Luders, G. P. Souza, N. M. Kimura, and A. J. Palangana, Cryst. Res. Technol. **44**, 1255 (2009).

[16] P. K. Mukherjee and K. Sen, J. Chem. Phys. **130**, 141101 (2009).

[17] S. Romano and G. de Matties, Phys. Rev. E **84**, 011703 (2011).

[18] M. J. Freiser, Phys. Rev. Lett. **24**, 1041 (1970).

[19] M. Dijkstra, R. van Roij, and R. Evans, Phys. Rev. E **63**, 051703 (2001).

[20] A. Poniewierski and R. Hołyst, Phys. Rev. A **38**, 3721 (1988).

[21] H. Reich and M. Schmidt, J. Phys.: Condens. Matter **19**, 326103 (2007).

[22] T. Geigenfeind, S. Rosenzweig, M. Schmidt, and D. de las Heras, J. Chem. Phys. **142**, 174701 (2015).

[23] R. Zwanzig, J. Chem. Phys. **39**, 1714 (1963).

[24] S. Dietrich, in *Phase Transitions and Critical Phenomena*, edited by C. Domb and J. L. Lebowitz (Academic, London, 1988), Vol. 12.

[25] Y. Martinez-Raton, S. Varga, and E. Velasco, Phys. Chem. Chem. Phys. **13**, 13247 (2011).

[26] M. Gonzalez-Pinto, Y. Martinez-Raton, and E. Velasco, Phys. Rev. E **88**, 032506 (2013).

[27] M. C. Lagomarsino, M. Dogterom, and M. Dijkstra, J. Chem. Phys. **119**, 3535 (2003).

[28] E. Van den Pol, A. V. Petukhov, D. M. E. Byelov, and G. J. Vroege, Phys. Rev. Lett. **103**, 258301 (2009).

[29] E. Van den Pol, D. M. E. Thies-Weesie, A. V. Petukhov, D. V. Byelov, and G. J. Vroege, Liq. Cryst. **37**, 641 (2010).

[30] G. J. Vroege, Liq. Cryst. **41**, 342 (2014).

[31] K. Slyusarenko, D. Constantin, and P. Davidson, J. Chem. Phys. **140**, 104904 (2014).

[32] S. Belli, A. Patti, M. Dijkstra, and R. van Roij, Phys. Rev. Lett. **107**, 148303 (2011).

[33] A. B. G. M. L. Reinink, S. Belli, R. van Roij, M. Dijkstra, A. V. Petukhov, and G. J. Vroege, Soft Matter **10**, 446 (2014).